SIMULATION INVESTIGATION OF SAFETY LIMITS OF HELICOPTER OPERATIONS

Jarosław Stanisławski, email: jaroslaw.stanislawski@ilot.edu.pl, Institute of Aviation (Poland)

Abstract

The paper presents results of simulations concerning some aspects of helicopter operation safety which include the H-V zone limits, loss of tail rotor aerodynamic effectiveness, operations of ship-borne helicopter and maneuver flight. For simulation investigation, two kinds of physical models of helicopter with different simplification level of real rotorcraft structure are applied. For analysis of emergency situation after power loss, the helicopter is treated as point mass of fuselage suspended beneath main rotor in form of non-deformable disk area. To define the rotor loads and blade deflections generated in boundary flight states a more precise model of elastic blades is applied which consists of deformable blade axes with sets of lumped masses distributed along blade radius. The axis model allows flap, lead-lag and pitch motion of blade. Equations of motion of rotor blades are solved applying Runge-Kutta method. Data of light helicopter were applied for simulations. The simulation investigation may help to collect data for prediction conditions of helicopter flight which can generate potentially dangerous situations.

1. INTRODUCTION

A high safety level for helicopter construction is considered as an important task for project team designing a new rotorcraft. Safety conditions should be preserved by flying crews and ground personnel during daily helicopter operations. Requirements in certification specifications define conditions of airworthiness of the helicopter. Despite fulfillment of the numerous regulations the complete elimination of accidents is not possible. Statistics concerning civil rotorcraft accidents which happened for long period of time can be found in reports[1] [2]. Information on accidents which have occurred lately are published in AAIB (Air Accident Investigation Branch) bulletins[3] and NTSB (National Transportation Safety Board) reports[4]. In many cases reasons of helicopter accidents could be directly connected with crew mistakes or poor recognition of arising dangerous situation. Flawed maintenance and inspection can also be pointed out as risk factor in helicopter accidents[5].

Helicopter certification procedures demand to define the limits of H-V zones which are also called the dead-man curves. For multi-engine helicopters in the case of OEI (one engine inoperative) the rest of available power may be enough to perform emergency maneuver of flight continuation. The H-V zones define the values of flight velocity and height in the vicinity of ground where in the case of power loss a safety autorotation landing is impossible to accomplish. The limits of the H-V zone include three branches the upper UHV, the lower LHV and velocity limit VHV.

The range of H-V zones limits strongly depends on mass of helicopter and height of landing surface[6]. Potentially dangerous values of velocity and height of flight depend on the level of power loss, the mass of helicopter, the height above sea level of landing area and also on proper reaction of the pilot. The task of helicopter landing after power loss can be treated as an optimal control problem[7], [8],[9].

Due to progress in electronic technology, realization of an airborne device including module with code computing in accelerated rate of time may help pilot to get exact information on actual envelope of H-V zone and cue the control input for execution emergency maneuver after power loss[10].

Presented in this paper results of simulation of H-V zone concern data of hypothetical light helicopter with four-bladed main rotor. Plots of H-V zones show large differences due changes of flight parameters possible to occur in normal operation of helicopter. The home-code program applying the point mass model of helicopter was used for calculations in accelerated rate of time the range of H-V zones . Presentation of changing H-V zone limits and prediction of control function may be crucial importance for pilot to make the proper decision in condition of time deficiency in the case of power loss.

The more precise calculation model was applied for simulation behavior of the main rotor blades or the tail rotor blades in circumstances which may lead to generate potentially danger situations during hover or slow flight in vicinity of ground. In some helicopter flight conditions the phenomenon of loss of tail rotor aerodynamic effectiveness (LTE) can occur. Other situations considered due to main rotor limitations include pull-up maneuvers or the case of ship-borne helicopter during take-off or landing on oscillating ship deck. The model of elastic blade consists of deformable axis with set of lumped masses distributed along blade radius (Fig.1).

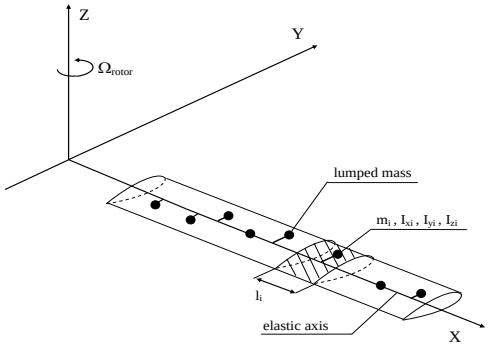

Fig.1. Elastic axis and lumped masses of blade.

Presented at 45th European Rotorcraft Forum, Warsaw, Poland, 17-20 September, 2019

Introducing as program input data the aerodynamic characteristics of blade airfoils due to attack angle and Mach number, calculations for simulated rotor revolution require time of few seconds. The model of deformable blade allows flap, lead-lag and pitch motion of blade including effects of out-of-plane and in-plane bending and torsion due to aerodynamic and inertial forces and moments acting on the rotor blades. Equations of motion of rotor blades are solved applying Runge-Kutta method. The calculated parameters of blade motion, according to Galerkin method, are considered as a combination of applied bending and torsion eigen modes of the rotor blade.

2. H-V ZONE

Considering H-V zones, flight safety can be increased by bringing to pilot in real time exact information on actual height required for eventual emergency maneuver. The algorithm for computing the parameters of emergency maneuver enables calculations of helicopter flight path for deficiency the available power in case of total or partial engines failure. The following simplifications are assumed to define the model of controlled flight of helicopter:

- only motion of helicopter in longitudinal plane is taken into consideration,
- helicopter is treated as a point mass ,
- required position of swash-plate is calculated for rigid rotor blades,
- emergency maneuver is divided for partial components with different limits of required flight parameters
- the operational limits such as: range and rate of deflection of the control system, allowed change of rotor speed, time of engine acceleration are considered,
- a time delay reaction of pilot reaction for engine failure is introduced.

The pilot action is modeled indirectly by calculating, at each time step of the simulated flight, the increments of horizontal Δa_x and vertical Δa_z accelerations of helicopter enabling realization the partial task at actual phase of maneuver. Next, according to the value of accelerations, the changes of collective and cyclic pitch are determined.

The vertical T_z and longitudinal T_x components of rotor thrust in flight at speed V and acceleration a_z , a_x are following:

(1) $$T_Z = mg + ma_Z \quad ,$$

(2) $$T_X = ma_X + \frac{1}{2}\rho V^2 S C_X \quad .$$

The thrust vector is assumed to be close orientated to rotor shaft axis, so the fuselage pitch angle φ_y can be estimated as

(3) $$\gamma \approx \frac{T_X}{T_Z} \approx \varphi_y \quad ,$$

γ - tilt of rotor thrust .

Power necessary to drive rotor P_{rotor} can be define as function of thrust coefficient c_T^*, rotor inflow λ_T and advance ratio μ_T due to blade tip plane

(4) $$P_{rotor} = f(c_T^*, \lambda_T, \mu_T) \quad .$$

The change of rotor rotational speed $\dot{\Omega}$ demands increase of the total required power

(5) $$P_{req} = \frac{P_{rotor}}{\xi} + \frac{I_0 \dot{\Omega} \Omega}{\xi} \quad ,$$

ξ – power efficiency factor, I_0 –rotor inertia moment.

The blade collective pitch ϑ_o is calculated as function which depends on values of rotor thrust coefficient c_T^*, rotor inflow λ_T and advance ratio μ_T , blade twist ϑ_{twist} and γ longitudinal tilt of rotor

(6) $$\vartheta_o = f(c_T^*, \lambda_T, \mu_T, \gamma, \vartheta_{twist}) \quad .$$

For state of flight with acceleration a_z the values of rotor thrust T power P and collective pitch ϑ_o can be found. Introducing the unitary increasing impulse of acceleration Δa_{z1}

$$\Delta a_{z1} = a_{z1} - a_z = 1$$

enables to obtain the new value of rotor thrust T_1 power P_1 and collective pitch ϑ_{o1} required to fulfill the condition of enlarged acceleration. The approximate derivatives of thrust, power and collective pitch with respect to acceleration impulse are defined as:

(7a) $$\frac{\Delta T}{\Delta a_{z1}} = T_1 - T \quad ,$$

(7b) $$\frac{\Delta P}{\Delta a_{z1}} = P_1 - P$$

(7c) $$\frac{\Delta \vartheta_0}{\Delta a_{z1}} = \vartheta_{01} - \vartheta_0 \quad .$$

For limitations concerning maximum available power, critical thrust, maximum blade pitch the maximum acceleration impulses possible to achieve are determined:

- for power limit

(8a) $$\Delta a_{zP} = (P_{maks} - P) \cdot \frac{\Delta P}{\Delta a_{z1}} \quad ,$$

- for thrust limit

(8b) $$\Delta a_{zT} = (T_{KR} - T) \cdot \frac{\Delta T}{\Delta a_{z1}} \quad ,$$

- for blade pitch limit

(8c) $$\Delta a_{z\vartheta_0} = (\vartheta_{0\,maks} - \vartheta_0) \cdot \frac{\Delta \vartheta_0}{\Delta a_{z1}} \quad .$$

Selection the least value Δa_{zmin} among acceleration impulses defined by equations (8) allows in next time step $t+\Delta t$ to perform controlled flight within all limits for changed components of helicopter acceleration

(9) $$a_{z\,t+\Delta t} = a_{z\,t} + \Delta a_{z\,\min} \quad ,$$

the horizontal acceleration a_x is coupled as following

(10) $$a_x = (a_z + g) \cdot \sin\varphi_y \quad ,$$

φ_y – angle of helicopter pitch.

Repeating calculation for the next time steps Δt the flight path and velocity of helicopter can be determined as follows:

Presented at 45th European Rotorcraft Forum, Warsaw, Poland, 17-20 September, 2019

(11a) $$x_{i+1} = x_i + v_i \cdot \Delta t + \frac{a_{xi} \cdot \Delta t^2}{2} \quad ,$$

(11b) $$v_{i+1} = v_i + a_{xi} \cdot \Delta t \quad ,$$

(11c) $$z_{i+1} = z_i + w_i \cdot \Delta t + \frac{a_{zi} \cdot \Delta t^2}{2} \quad ,$$

(11d) $$w_{i+1} = w_i + a_{zi} \cdot \Delta t \quad .$$

Results of H-V zones simulation, shown in Fig.2, concern a hypothetical twin engine light helicopter in the case of total power loss. Differences in range of H-V zones which can be noticed for upper branch UVH, depend mainly on mass of helicopter.

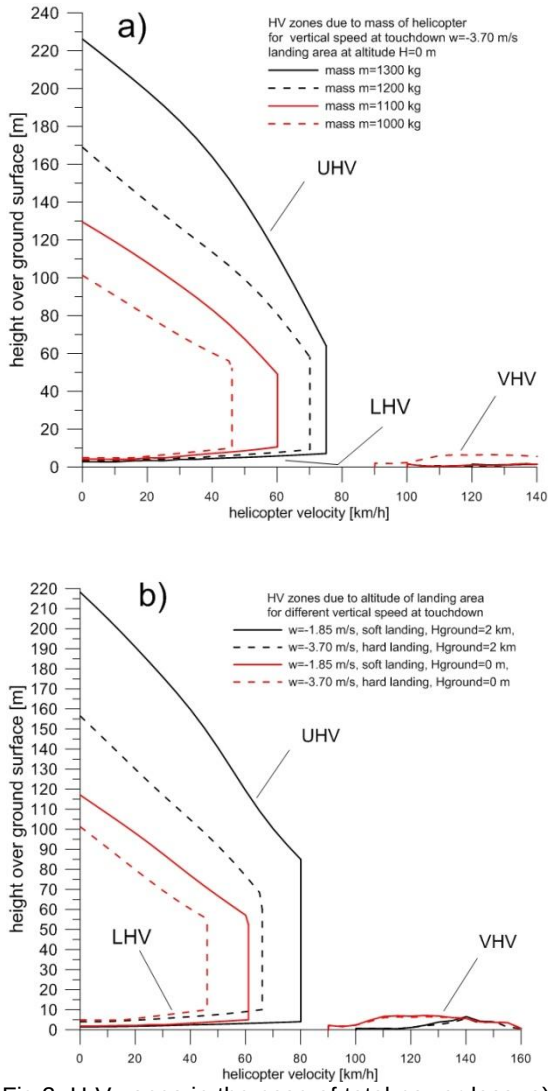

Fig.2. H-V zones in the case of total power loss: a) due to helicopter mass, b) due to altitude of landing area and allowed vertical speed at moment of touchdown.

. If total power loss occurs in hover above landing area at sea level (Fig.2a) the excess altitude, necessary to perform safety autorotation landing with allowable vertical speed at touchdown, will vary from 100m for helicopter mass equals 1000kg to over 220m for mass of 1300kg. The plots in Fig.2b show the changes of H-V zones for helicopter mass of 1000kg due to other conditions like altitude of landing area and vertical speed at moment of touchdown for soft or hard landing. It is worth to noticed that for the power loss in hover at altitude of 2 km the excess height arises nearly to 220m for emergency maneuver with condition of soft landing (w= -1.85m/s). The high value of height loss in emergency maneuver in the case of total power loss in hover is connected with mutual necessity to sustain rotor rotation and to increase velocity of helicopter flight. Along with higher velocity at moment of power loss the emergency maneuvers are enabled for lower excess of height.

In Fig.3 are shown the run-time plots emergency maneuver parameters after total power loss in hover for helicopter of 1000kg mass. For assumed lack of pilot reaction during the first second after failure of engines the quick decreasing rate of the main rotor speed is observed. In the next phase of maneuver pilot tried to restore rotor speed to nominal value which was achieved due to loss of flight height with simultaneous increase of helicopter velocity. In flare, the last phase of maneuver the descent speed of helicopter is reduced to allowed value as result of decrease rotor rotation. The whole maneuver lasted about 10 seconds and required level distance of 60m and excess height of 100m.

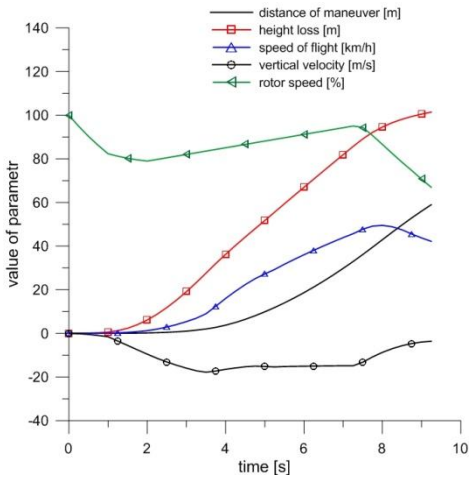

Fig.3. Simulation of emergency maneuver after total power loss in hover for helicopter of 1,000 kg mass, vertical velocity at touchdown w=-3.70 m/s.

In Fig.4 are shown results of the emergency maneuver simulations for the cases of partial power loss(OEI) for which failure occurred in hover condition. The possible to achieve ascent velocity of flight strongly depends on mass helicopter (Fig.4a). The plots for helicopter mass of 1300kg and 1500kg show the value of horizontal velocity to which helicopter should be accelerated to continue the level flight despite available power only of one engine operative - feature of the Category A class helicopter. For the overloaded helicopter with mass of 1700kg power of one engine is too low for level flight continuation. In Fig.4b can be noticed that excess of height required to achieve level flight in OEI condition increases with mass of helicopter.

Presented at 45th European Rotorcraft Forum, Warsaw, Poland, 17-20 September, 2019

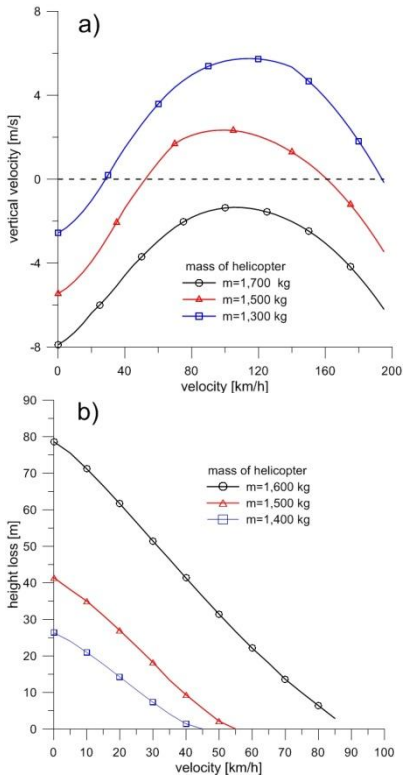

Fig.4. Emergency maneuver in the case of one engine inoperative (OEI) in hover due to helicopter mass: a) possible to achieve vertical velocity of flight, b) height loss in emergency maneuver for flight continuation

3. LOSS OF TAIL ROTOR EFFECTIVENESS

A phenomenon of loss of tail rotor aerodynamic effectiveness (LTE) are observed for coincidence of following circumstances: helicopter in hover or closed to it in flight at low height and low speed with occurrence the wind blowing from direction disturbing an airflow of tail rotor. In Fig.5 are shown the situations for which the wind direction may influence on reduction the tail rotor efficiency.

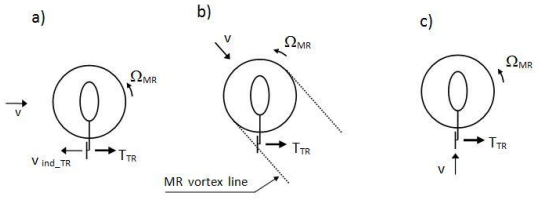

Fig.5. Flight conditions when aerodynamic effectiveness loss of tail rotor could be observed (TR - tail rotor, MR - main rotor) : a) side flight, wind gusts, b) flight in range of directions where interference of the main rotor wake may occur c) backward flight.

As reaction on high rate of the helicopter accidents which can be associated with loss of directional control the American FAA issued Advisory Circular 90-95[11] with description of the phenomenon of aerodynamic effectiveness loss of the tail rotor and collecting the recommendations and instructions for pilots to avoid the potentially dangerous situations.

Information on circumstances of increased possibility of the effectiveness loss of tail rotor were also collected in EASA documents concerning safety of flight[12], [13] and edited by FAA in rotorcraft flying handbook[14].

Presented in this paper results of simulation concern work of tail rotor of light helicopter in the case of the level flight at low speed for which the main rotor vortex, generated in the vicinity of ground, passes through the tail rotor area.

The helicopter model applied for the tail rotor simulation includes following components:

- the stiff fuselage with motion diminished to yaw around the axis of the main rotor shaft,
- the tail rotor treated as set of elastic blades (Fig.1) with possibility of introducing the function of blade pitch control,
- for conditions of forward flight the simplified model of the main rotor wake applied in form of two vortex lines generated behind the main rotor (Fig 5b).

Taken under consideration simulation of directional maneuver of helicopter the simplified equation of rotation motion of fuselage is as follows:

$$I\ddot{\beta}_f = M_{mr} + M_f + T_{tr} \times L_{tr} + M_{ytr} \quad (12)$$

where

I - fuselage moment of inertia relative to axis of the main rotor shaft,

M_{mr} - torque of the main rotor,

$M_f(\beta_f)$ - fuselage yawing aerodynamic moment,

$T_{tr}(\beta_f,\varphi)$ - tail rotor thrust,

$M_{ytr}(\beta_f,\varphi)$ - yawing moment of the tail rotor hub,

β_f - yawing angle of the fuselage,

φ - pitch angle of the tail rotor blades.

The model of the tail rotor blade, as shown in Fig.1, is treated as a structure which consists of elastic axis with distribution of lumped masses. Solution of the equations of motion of elastic blades takes into account mutual twist, bent in-plane and bent out-of-plane deflections of blade elastic axes. The equations of blade motion are solved using Runge-Kutta method. According to Galerkin method it is assumed that deflections of the elastic axis *y, z, φ* are equal to superposition of modal components deriving from considered eigen modes of tail rotor blade:

$$y(x,t) = \sum_{i1=1}^{I1} \rho_{i1}(t) y_{i1}(x), \quad (13a)$$

$$z(x,t) = \sum_{i2=1}^{I2} \delta_{i2}(t) z_{i2}(x), \quad (13b)$$

$$\varphi(x,t) = \sum_{i3=1}^{I3} \eta_{i3}(t) \varphi_{i3}(x), \quad (13c)$$

where

y_{i1}, z_{i2}, φ_{i3} - eigen modes respectively in-plane, out-of-plane bending and torsion;

ρ_{i1}, δ_{i2}, η_{i3} - time dependent shares of each eigen mode determined in computing process;

I1, I2, I3 - numbers of considered bending and torsion eigen modes.

Applying orthogonality condition for the eigen modes equation of motion of elastic blade can be converted into sets of equations (14), where each equation can be treated as equation of oscillating motion of an equivalent structure with a single degree of freedom. The frequencies of considered eigen modes of blade

Presented at 45th European Rotorcraft Forum, Warsaw, Poland, 17-20 September, 2019

are equal respectively frequencies of eigen modes of equivalent structures:

(14a) $\ddot{\rho}_{i1} + \rho_{i1} p_{i1}^2 = Q_{Y_{i1}}$, i1 = 1,..., I1

(14b) $\ddot{\delta}_{i2} + \delta_{i2} f_{i2}^2 = Q_{Z_{i2}}$, i2 = 1,...,I2

(14c) $\ddot{\eta}_{i3} + \eta_{i3} \nu_{i3}^2 = Q_{\varphi_{i3}}$, i3 = 1,...,I3

where

p_{i1}^2 , f_{i2}^2 , ν_{i3}^2 - square of blade eigen mode frequencies for bending in-plane, out-of-plane and torsion,

$Q_{Y_{i1}}, Q_{Z_{i2}}, Q_{\varphi_{i3}}$ - generalized forces for considered eigen modes of the tail rotor blade.

For given moment of time the parameters of blade motion are determined as sum of contributions (13) of considered blade eigen modes. Aerodynamic forces acting on segment of blade at given azimuth position on the tail rotor disk are computed applying the blade element theory. The local angle of attack at blade cross-section depends on temporary conditions of airflow:

(15) $\alpha = \vartheta_{contr} + \varphi_g + \Delta\varphi - arc\,tg\left(\frac{u_Z}{u_X}\right)$,

where

ϑ_{contr} - pitch angle due to control,

φ_g - geometric twist,

$\Delta\varphi$ - torsion deformation,

u_z, u_x - components of airflow at cross-section of the tail rotor blade: out-of-plane and in-plane.

The equations of motion of elastic tail rotor blades are solved with time step coincident with change of the azimuth position of blade at the tail rotor disk equals angle $\Delta\psi = 5^o$

The velocity induced by the main rotor wake may strongly affects the airflow components of the tail rotor blades. In vicinity of ground in condition of hover with wind or low-speed flight the horseshoe wake of the main rotor is simplified to form which consists of two vortex lines located behind the main rotor (Fig.5b). The distribution of velocity induced by vortex lines is defined applying the Biot-Savart law.

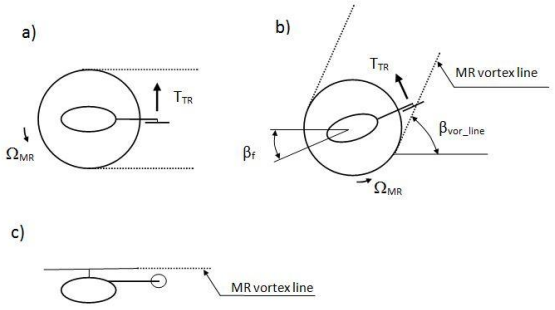

Fig.6. Scheme of position of the main rotor vortex line relative to tail rotor: a) upper view - initial position of fuselage and vortex lines, b) upper view - vortex line is passing through plane of tail rotor of turning helicopter, c)side view - vortex line above tail rotor disk.

The simulation test concerns the case of helicopter in hover with assumed the passage of the main rotor vortex line nearby the tail rotor disk. The vortex line is thought to approach gradually to the tail rotor area passing over its disk (Fig.6).

The vortex line treated as stiff is changing its angle position at rate of $0{,}01^o$ for one step of tail rotor blade azimuth change $\Delta\psi = 5^o$, which corresponds to the increment of position angle of the vortex line $\Delta\beta_{vor\_line} = 0{,}72^o$ for one revolution of the tail rotor shaft. The simulation started with the main rotor vortex line in the parallel position to the longitudinal axis of the fuselage. After 100÷130 revolutions of the tail rotor (time of simulation 1,5÷1,95 s) the vortex line passed nearby the tail rotor disk over blade tips at its high position.

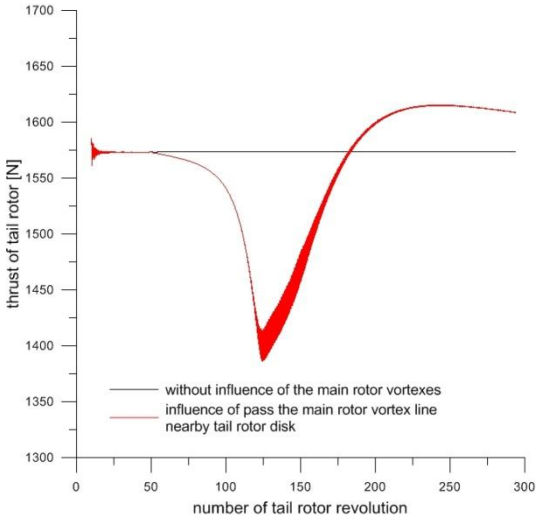

Fig.7. Changes of tail rotor thrust in hover, with blade pitch kept constant, for case of passing the main rotor vortex line in vicinity of tail rotor disk.

In Fig.7 is shown the comparison the time-run plots of the tail rotor thrust in hover. For the case without influence of the main rotor vortexes the value of tail rotor is constant. In the second case the main rotor vortex line passed in vicinity of the tail rotor. The rapid changes of tail rotor thrust can be observed between 100th÷150th of rotor revolutions. In both cases of simulation the tail rotor blade pitch was kept at the same, steady level (Fig.8a). The diminished tail rotor thrust was not enough to counteract main rotor torque so, with assumed lack of pilot reaction, helicopter started the rotation motion (Fig.8a,b). The decrease of thrust can be connected with disturbances of airflow velocity generated by the main rotor vortex line which approached vicinity of the tail rotor disk. The changes of tail rotor blades airflow components generated in-plane and out-of-plane of the tail rotor during passage of the main rotor vortex line are presented in Fig.9a,b.

The influence of disturbances in the tail rotor blades airflow components can be noticed at time-run of blade attack angle (Fig.10). In Fig.11a is shown fragment of time-run of attack angle at tail rotor blade tip for range of the 120th-130th revolutions for which position of main rotor vortex line is found very close to tail rotor disk. For tail rotor revolution the rapidly decrease of attack angle

Presented at 45th European Rotorcraft Forum, Warsaw, Poland, 17-20 September, 2019

at blade tip can be noticed when tail rotor blade approaches its high position at azimuth 270^o in tail rotor disk (Fig.11b). The sharp changes of attack angle cause the increased level of blade torsion oscillation. In Fig.12a is presented the plot of torsion deflection at tip of tail rotor blade for the 120th-130th revolutions. The distribution of blade torsion deflection for the 125th revolution of tail rotor (Fig.12b) shows oscillations reaching peak-to-peak over 2^o at blade tip. The frequency of torsion oscillations observed in Fig.12b is close to frequency of torsion eigen mode of tail rotor blade applied as input data for simulation program code.

a)

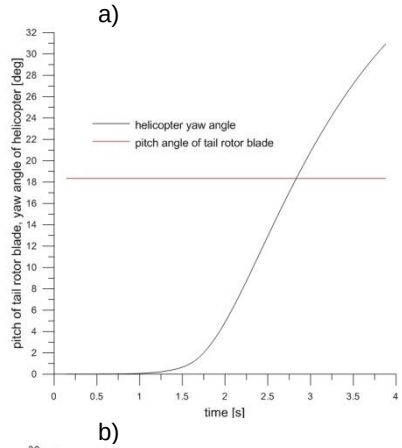

b)

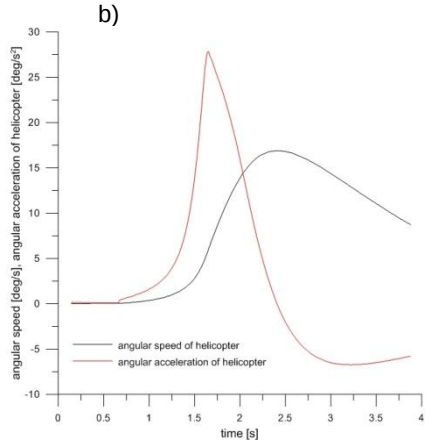

Fig.8. Yaw angle (a), acceleration and angular speed (b) of helicopter during passing the main rotor vortex line in vicinity of tail rotor disk with assumed lack of action of pilot (constant pitch of tail rotor blades)

a)

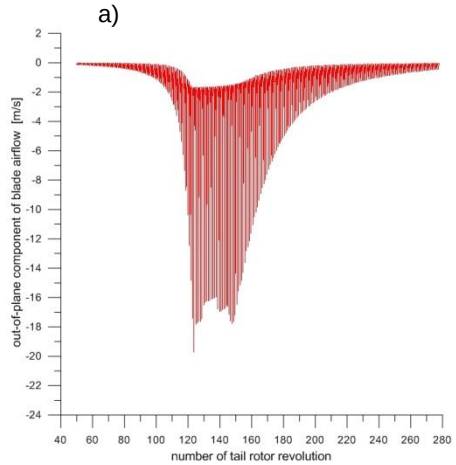

b)

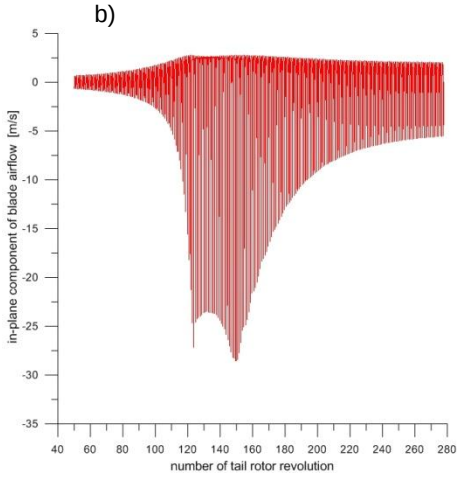

Fig.9. Components of airflow at tip of tail rotor blade in hover during passing the main rotor vortex line in vicinity of tail rotor disk, assumed constant pitch of tail rotor blades:
a) component out of tail rotor plane, (-) direction coincident with induced velocity of tail rotor reducing attack angle of tail rotor cross-section,
b) component in tail rotor plane, (-) direction coincident with rotation of blade causing reduction of its airflow speed.

The influence of disturbances in the tail rotor blades airflow components can be noticed at time-run of blade attack angle (Fig.11).

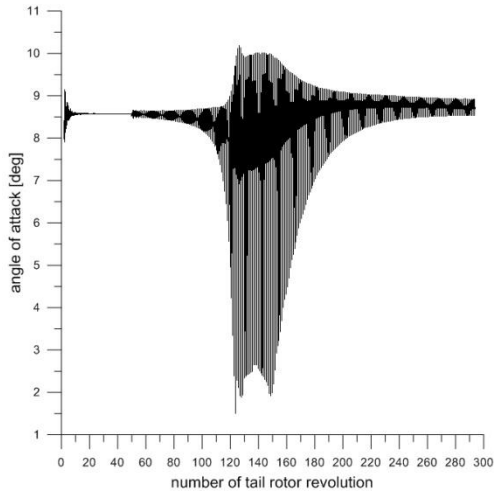

Fig.10. Angle of attack at tip of tail rotor blade in hover during passing the main rotor vortex line in vicinity of tail rotor disk with assumed constant pitch of tail rotor blades.

In Fig.12a is shown fragment of time-run of attack angle at tail rotor blade tip for range of the 120th-130th revolutions for which position of main rotor vortex line is found very close to tail rotor disk. For tail rotor revolution the rapidly decrease of attack angle at blade tip can be noticed when tail rotor blade approaches its high position at azimuth 270^o in tail rotor disk (Fig.12b). The sharp changes of attack angle cause the increased level of blade torsion oscillation. In Fig.13a is presented the plot of torsion deflection at tip of tail rotor blade for the 120th-130th revolutions. The distribution of blade

Presented at 45th European Rotorcraft Forum, Warsaw, Poland, 17-20 September, 2019

torsion deflection for the 125th revolution of tail rotor (Fig.13b) shows oscillations reaching peak-to-peak over 2^{o} at blade tip. The frequency of torsion oscillations observed in Fig.13b is close to frequency of torsion eigen mode of tail rotor blade applied as input data for simulation program code.

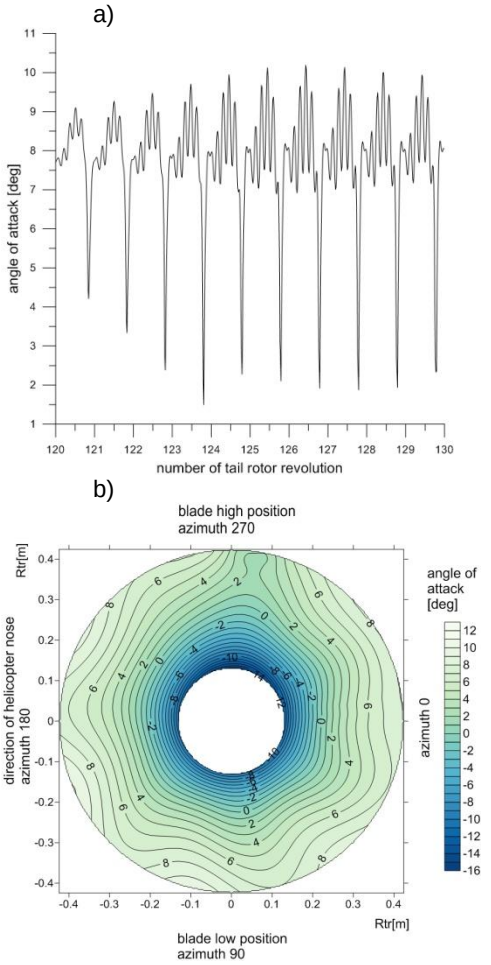

Fig.11. Time run of attack angle (a) at tip of tail rotor blade, fragment of simulation for 120th-130th revolutions of tail rotor during pass of main rotor vortex line nearby tail rotor disk. Map of attack angle distribution on tail rotor disk (b) for 125th revolution of tail rotor.

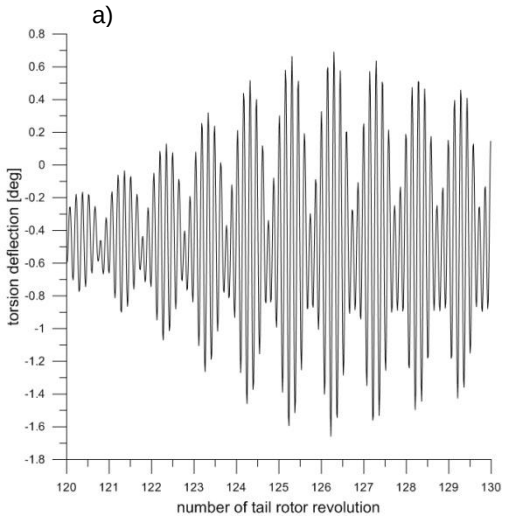

b)

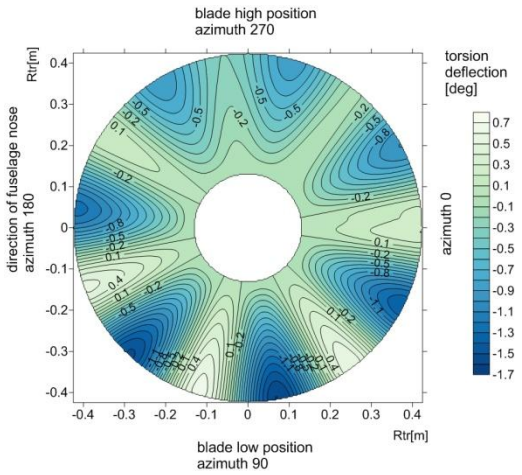

Fig.12. Time run of torsion deflection (a) at tip of tail rotor blade, fragment of simulation for 120th-130th revolution of tail rotor during pass of main rotor vortex line nearby tail rotor disk. Map of blade torsion deflection on tail rotor disk (b) for 125th revolution of tail rotor.

4. MAIN ROTOR BEHAVIOR

Behavior of main rotor is presented for two quite different cases of helicopter operation, for landing on deck of ship and for pull-up maneuver. Offshore helicopter operations generate more potentially dangerous circumstances in comparison to flights over land. A ship-board landing and take-off may become hazardous, especially in poor weather conditions when small area of flight deck in vicinity of obstacles of ship structure and motion of ship deck increase the risk level of ship-board helicopter operation. Problems of offshore helicopter transport in North Sea area and accidents in period of nearly forty years were analyzed in review prepared by UK Civil Aviation Authority[15]. In the US Coast Guard manual[16] are collected instructions for safe procedures of shipboard helicopters operation concerning limitations of ship roll, type of helicopter, size of ship and use of the special helicopter deck lock tie-down system. In NATO publication on helicopter ship qualification tests[17] are defined the rules of proper helicopter usage on ship board which point out dangerous situations like: blade sailing, strong tail wind or wind area of inadequate helicopter yaw control.

The model applied for simulation assumes that helicopter stands on ship-deck at the phase of take-off or landing when rotating rotor generate thrust less than weight of helicopter. The oscillating motion of ship deck due to waves is introduced. The model of helicopter consists of the main rotor with elastic blades (Fig.1) and fuselage treated as stiff body supported by spring-damper units which correspond to characteristics of landing gear. The scheme of displacements of rotor hub due to ship and helicopter fuselage motion is shown in Fig.13. The dynamic effects related to ship deck motion and fuselage motion due to deflections of landing gear units were added to the equations of motion of elastic rotor blades. The considered situations include the case

Presented at 45th European Rotorcraft Forum, Warsaw, Poland, 17-20 September, 2019

for nominal rotor speed with rotor thrust equals to 40% of helicopter weight and the case of reduced rotor speed to 30% of nominal value for which the blade hit to flap limiter can occur. The simulations were performed for data of the four-bladed light helicopter for periods of time equal to 100 revolutions of the main rotor. All cases of the calculations were executed under scheme which assumed that the first 10 rotor revolutions were devoted for the decay of initial conditions at fixed position of the rotor shaft. At the 10th revolution the helicopter motion on flexible landing gear units was allowed and after the 20th rotor revolutions, an option of ship motion was introduced.

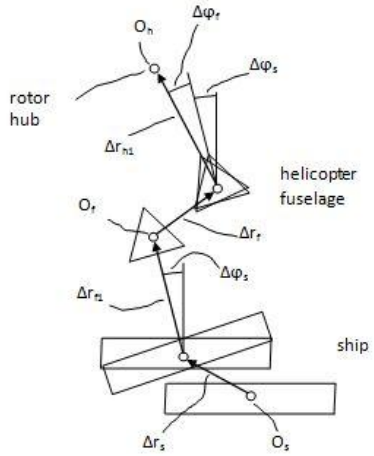

Fig.13. Scheme of displacements of rotor hub due to ship and fuselage motion.

Shown in Fig.14 plots of the main rotor blade flapping angle concern the case of helicopter staying on the ship deck which is assumed to perform motion of rolling oscillation as follows $\varphi_{x\text{-}ship}=8^{o}*\sin(0{,}8*t)$.

The main rotor rotates with nominal speed (100%) and the swashplate is kept in perpendicular position relative to rotor shaft axis. For windless condition (Fig.14a) the blade flapping angle diminishes for ranges of time when rolling angular speed of ship deck takes low value close to zero.

The blowing wind (Fig.14b) changes the attack angles of rotor blades which results in different and higher range of blade flapping. For the case of rotor speed reduced to 30% of nominal value due to diminished centrifugal forces, the blade flapping of increased value is observed (Fig.15). For higher amplitude of ship motion (Fig.15b) the blade flapping arises so much that for blade falling down the hits to the rotor hub limiter of flap angle occur. The blade and limiter contacts can be noticed as steady sections of run time with limited value, close to -4^{o} of flapping angle (Fig.15c).

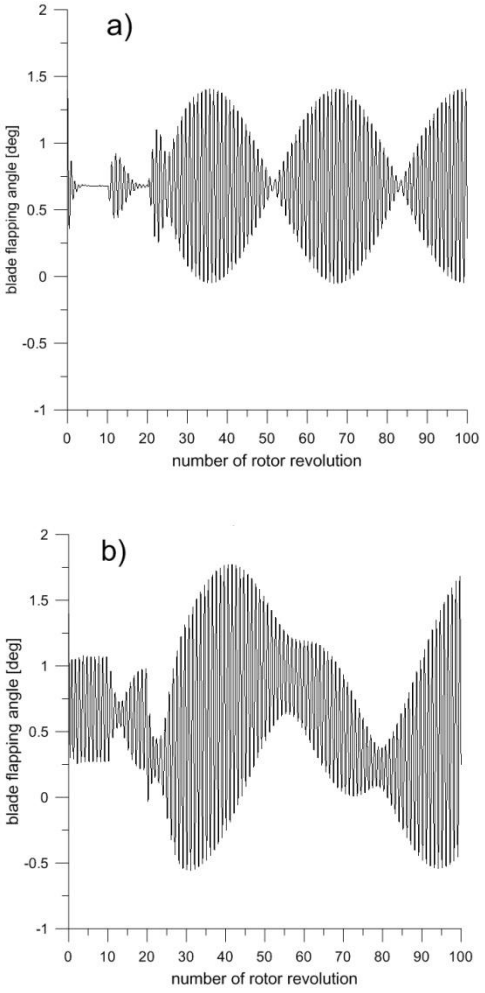

Fig.14. Influence of wind on blade flap angle at nominal rotor speed for helicopter standing on deck of rolling ship :
a) no side wind V_w= 0 m/s,
b) left side wind V_w= 15 m/s

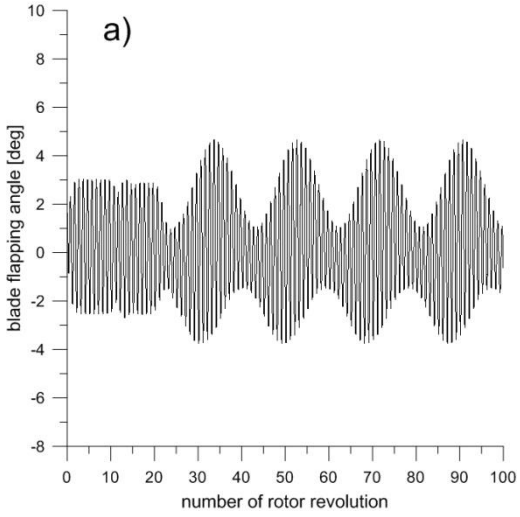

Presented at 45th European Rotorcraft Forum, Warsaw, Poland, 17-20 September, 2019

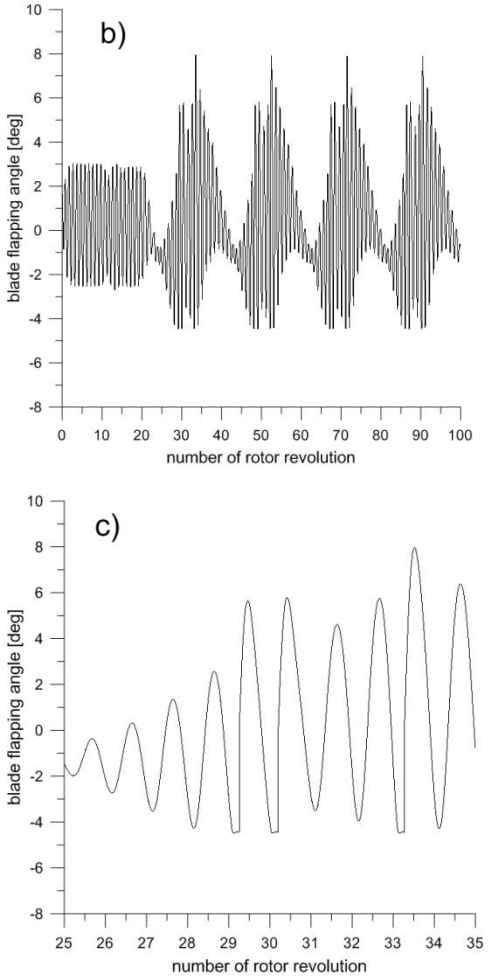

Fig.15. Blade flap angle for helicopter standing on ship deck due to amplitude of rolling motion of ship, rotor speed reduced to 30% of nominal value, side wind V_w=15 m/s, a) solution for lower 4^o amplitude of ship rolling, b) the case for higher, equal to 8^o, amplitude of ship motion, c) fragment of plot Fig.15b from 25^{th} to 35^{th} rotor revolution

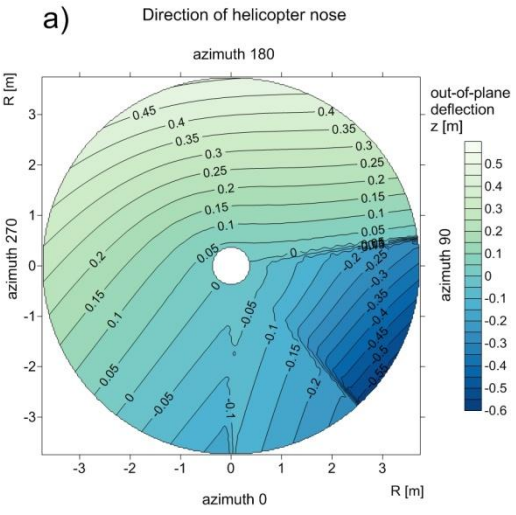

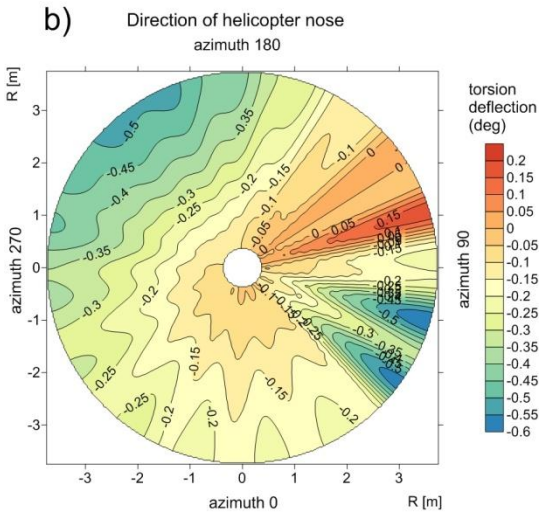

Fig.16. Rotor disk distribution of blade deflections during the 33^{rd} rotor revolution (see Fig.15c) in the case of blade hit to flap limiter: a) out-of-plane bending deflection, b) torsion blade deflection

The blade hit and the following contact with flap limiter affect boundary conditions of blade and rotor hub connection which demands the change of applied eigen modes of blade for time continuation of contact.

The effects of blade contact with flap limiter are observed in rotor disk distributions of blade deflections (Fig.16). for the 33rd rotor revolution the rapid increased of out-of plane blade bending deflections are noticed between azimuth of 45^o and 90^o (Fig.16a). Initially after azimuth of 45^o the bending deflection at blade tip reaches level of -0.6 m lower than plane of rotor rotation. Simultaneously the blade torsion oscillations are generated (Fig.16b).

The blade hit to flap limiter is also shown in disk distribution of out-of-plane blade bending moment (Fig.17) for which the bending moments of high values are generated at sections located near the blade root. The plots of moment distributions along blade radius are shown in Fig.17b. Extremely high increase of bending moment is observed at blade root for initial phase of blade contact with flap limiter. Information concerning the conditions for which the excessive blade bending moments occur may affect limitation of safety helicopter operation.

The model of isolated rotor consisted of elastic blades (Fig.1) was applied to simulate rotor behavior in high speed flight. The calculations were performed for time equal 20 rotor revolutions in quasi-steady condition with steady deflection of swash-plate and position of main rotor axis. In Fig.18 are compared the results of last two rotor revolutions for flight at velocity of 180 km/h and for initial phase of soft and sharp pull-up maneuvers with different swash-plate deflection and position of rotor axis. In level flight condition the fuselage of helicopter was kept in position with pitched down nose, for soft pull-up fuselage took nearly horizontal position and for sharp pull-up the fuselage nose up position was assumed.

Presented at 45th European Rotorcraft Forum, Warsaw, Poland, 17-20 September, 2019

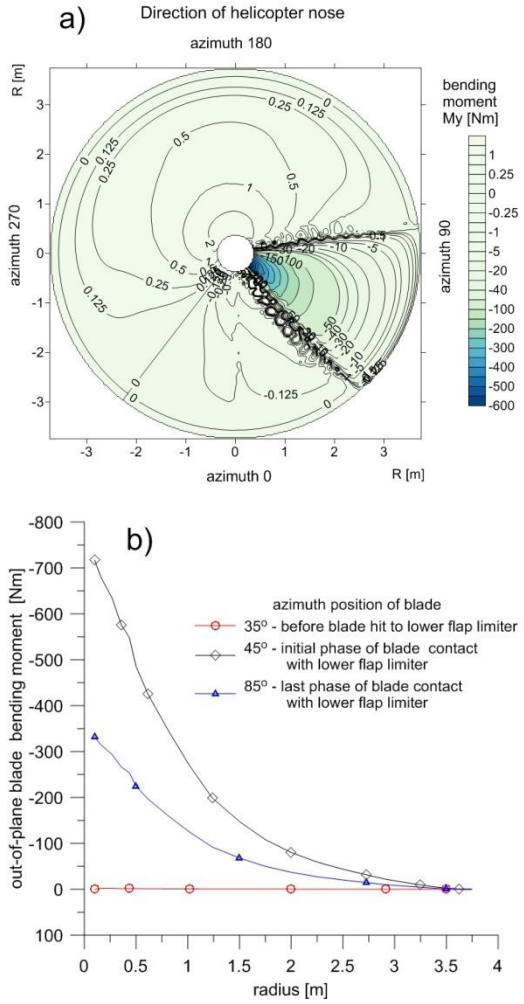

Fig.17. High rise of out-of-plane blade bending moment due to blade hit with flap limiter, results for the 33rd rotor revolution (see Fig.16c): a)moment distribution at rotor disk, b)moment along blade radius for selected azimuth positions

For pull-up maneuvers with tilted back rotor axis, the increased values of rotor thrust are generated (Fig.18a) and simultaneously the reduced power required to drive main rotor is noticed (Fig.18b). In Fig.18c for the case of sharp pull-up the oscillations of blade control moment appear.

The more detailed view of rotor air flow can be found in Fig.19÷21 in which are presented the rotor disk distributions of blade local attack angles and distributions of blade torsion deformations generated during the 20th rotor revolution.

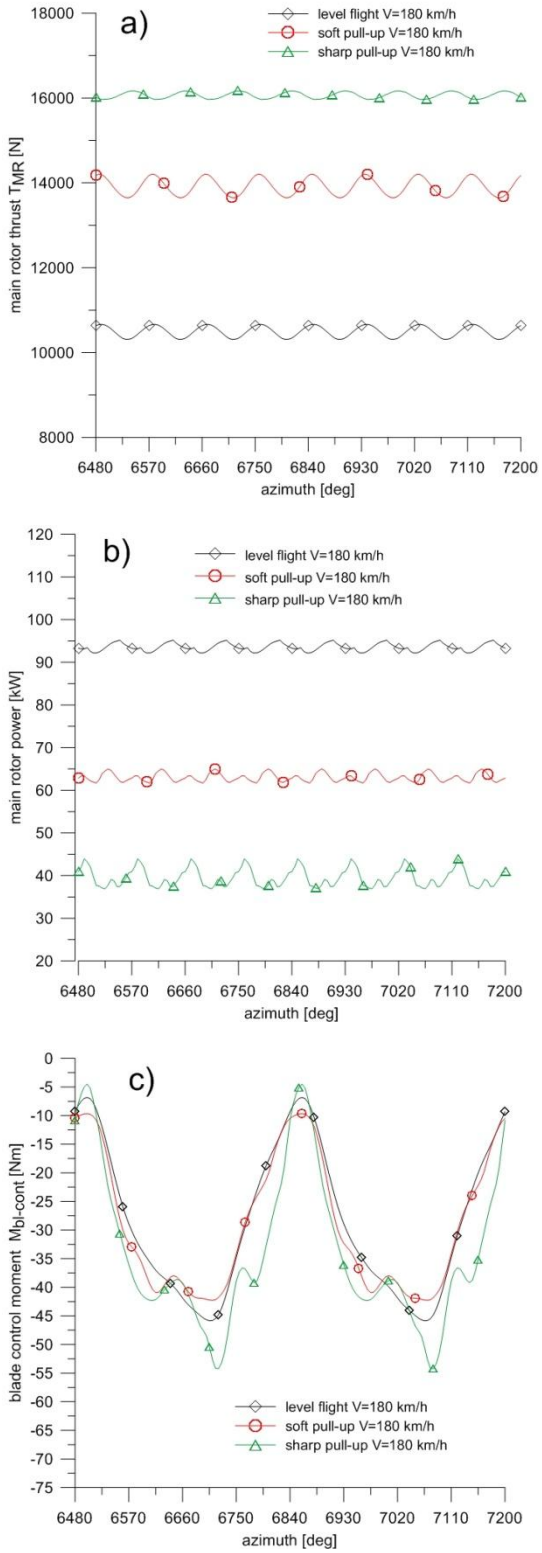

Fig.18. Loads of main rotor in level flight at velocity of V=180km/h and initial phase of soft and sharp pull-up maneuvers:

a) main rotor thrust,
b) power required to drive main rotor,
c) blade control moment

Presented at 45th European Rotorcraft Forum, Warsaw, Poland, 17-20 September, 2019

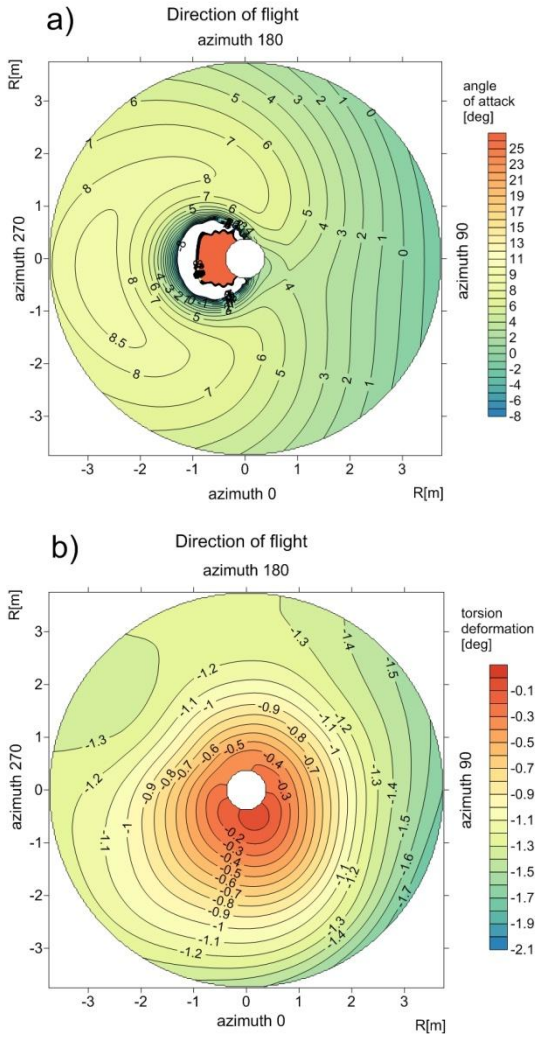

Fig.19. Rotor disk distribution of local attack angle (a) and distribution of blade torsion deformation (b) in level flight at velocity of V=180km/h with fuselage nose in down position.

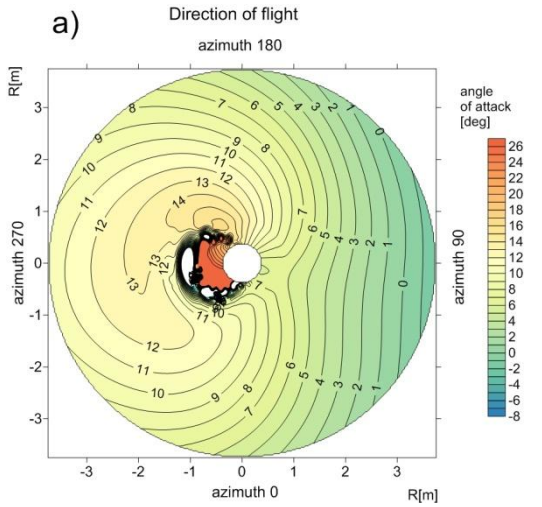

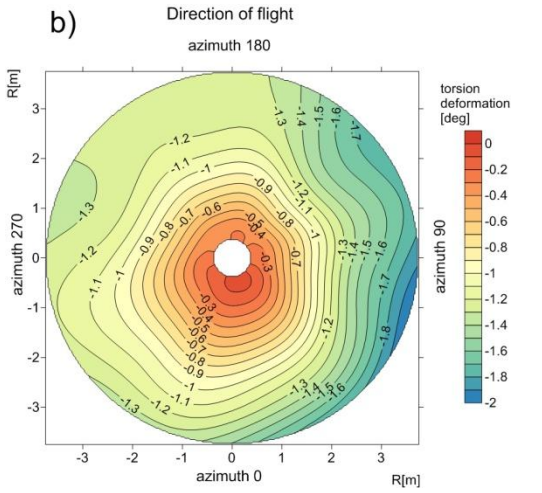

Fig.20. Rotor disk distribution of local attack angle (a) and distribution of blade torsion deformation (b) for soft pull-up at velocity of V=180km/h with fuselage nose close to horizontal position.

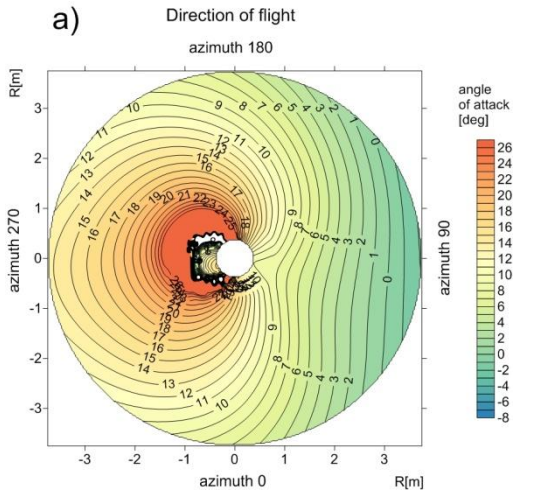

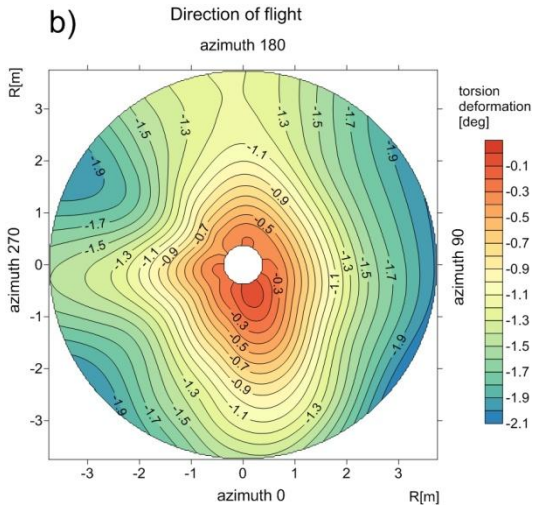

Fig.21. Rotor disk distribution of local attack angle (a) and distribution of blade torsion deformation (b) for sharp pull-up at velocity of V=180km/h with fuselage nose up position

Presented at 45th European Rotorcraft Forum, Warsaw, Poland, 17-20 September, 2019

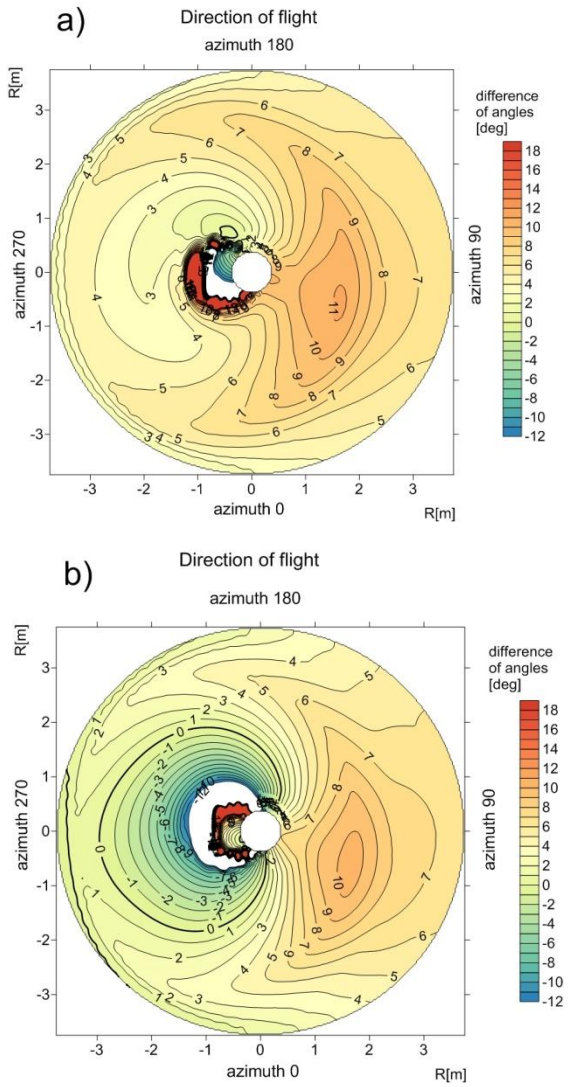

Fig.22. Comparison of rotor disk distributions of difference critical attack angle and local attack angle for soft (a) and sharp (b) pull-up maneuvers at velocity of V=180km/h

Comparing the distributions of attack angles, it is noticed that high values of attack angles appear for retreating blade at azimuthal position of 270°. For sharp pull-up the attack angles for retreating blade at top sections reach values of 14°÷16° (Fig.21a) in comparison of 8.5° for level flight conditions (Fig.19a). In the case of sharp pull-up the increase of attack angles is so high that large zone of separated airflow appears on rotor disk. In Fig.22b the zero izoline of distribution of difference critical attack angle and local attack angle shows the range of separated airflow zone. The rapid change of airflow conditions mutually generates oscillation of blade torsion deformation observed in Fig.21b. Blade passages through the zones of separated airflow cause the excessive increase of blade control moments (Fig.18c). Information on maneuvers generating high level loads may be useful for definition the limits of safety helicopter operation.

5. CONCLUSIONS

The computer simulation was applied for identification of circumstances and conditions which may lead to the potentially dangerous situations. The presented results of calculation concern some problems of helicopter safety operations, which include the H-V zone limits, loss of tail rotor aerodynamic effectiveness, landing or take-off operations of ship-borne helicopter, and pull-up maneuver limit in high speed flight. The simulations enable an analysis of conditions of helicopter operations and investigation of safe states limits of helicopter flight envelope.

The point-mass model of helicopter applied for H-V zones calculation enables execution of program code in accelerated rate of time. Implementation of the simulation program to cockpit device with graphical visualization of the calculated envelope of H-V zone may help pilot to prevent unnecessary operation inside H-V zone or in case of power loss may help to perform proper emergency maneuver.

The more detailed model of the elastic rotor blade was applied for calculation rotor loads and blade deformations to identify the circumstances for which negative phenomena may occur. The simulation program of directional maneuver in vicinity of ground allowed to define conditions of airflow disturbances generated by main rotor vortex lines which adverse affect the thrust of tail rotor.

The limits for helicopter operations on a ship deck can be defined considering the combined influence of wind condition, ship motion and range of rotor speed. The results of simulation determine conditions for which the excessive high level of blade loads can be generated during the helicopter operation on ship deck.

Simulations concerning pull-up maneuvers give some hints on rate control inputs which prevent generating the separated airflow zones at cross-sections of rotor blades.

The simulations of helicopter maneuvers can be useful for prediction the limits of safe helicopter operations.

REFERENCES

1. Harris F.D., Kasper E.F., Seler L.E.: *U.S. Civil Rotorcraft Accidents, 1963 Through 1997*, NASA TM-2000-209597, December 2000.
2. Liu L., Pines D.J.: Analysis of U.S. *Civil Rotorcraft Accidents Caused by Vehicle Failure or Malfunction, 1998-2004*, 61st Annual Forum of American Helicopter Society, Grapevine, Texas, June 1-3, 2005.
3. https://assets.publishing.service.gov.uk/government/uploads/system/uploads/attachment_data/file/749117/Bulletin_11-2018_Hi_Res.pdf
4. https://www.ntsb.gov/_layouts/ntsb.aviation/AccList.aspx?month=2&year=2019
5. Saleh J.H., Tikayat Ray A., Zhang K.S., Churchwell J.S., *Maintenance and inspection as risk factors in helicopters accidents: Analysis and recommendations*, PLoS ONE 14(2): e0211424, https://journals.plos.org/plosone/article?id=10.1371/journal.pone.0211424

Presented at 45th European Rotorcraft Forum, Warsaw, Poland, 17-20 September, 2019

6. Pegg J., *An Investigation of the Helicopter Height-Velocity Diagram Showing Effects of Density Altitude and Gross Weight*, NASA, TN D-4536, 1968
7. Zhao Y.J., Carlson E.B., Jhemi A.A., Chen R.T.N., *Optimization of Rotorcraft Flight in Engine Failure*, 56th Annual Forum of American Helicopter Society, Virginia Beach, Virginia, May 2-4, 2000.
8. Carlson E.B., Xue S., Keane J., Burns K., *UH-1 Upgrades Height-Velocity Diagram Development Through Flight Test and Trajectory Optimization*, 62nd Annual Forum of American Helicopter Society, Phoenix, Arizona, May 9-11, 2006.
9. Bibik P., Narkiewicz J., *Helicopter modeling and optimal control in autorotation*, 64th Annual Forum of American Helicopter Society, Montreal, Canada, April 29- May 1, 2008.
10. Stanisławski J., *Prediction of helicopter H-V zone and cueing the emergency maneuver after power loss,* The Archive of Mechanical Engineering, Vol.LVII, number 1, 2010.
11. Unanticipated Right Yaw in Helicopters (1995), *Federal Aviation Administration, Advisory Circular* No.90-95 issued 12/26/95.
12. Loss of tail rotor effectiveness (LTE) on unanticipated yaw in helicopters (2010), *EASA Safety Information Bulletin* No.2010-12R1 issued 21 October 2010.
13. Safety Considerations, *Training Leaflet HE1* (2010), EASA European Helicopter Safety Team (EHEST), October 2010.
14. *Rotorcraft Flying Handbook* (2000), Federal Aviation Administration, FAA-H-8083-21, Chapter 11.
15. Civil Aviation Authority, *Safety review of offshore public transport helicopter operations in support of the exploitation of oil and gas*, CAP 1145, 2014.
16. US Coast Guard, *Helicopter Operational Procedures Manual*, 2011.
17. NATO Research and Technology Organization, *Helicopter/Ship Qualification Testing*, RTO-AG-300, Flight Test Techniques Series, Vol.22, 2003.

Presented at 45th European Rotorcraft Forum, Warsaw, Poland, 17-20 September, 2019